



# In-situ Investigation of the Onset of Cavitation Damage from Single Bubbles on Technical Alloys

Jonas Kühlmann<sup>1</sup> · Christina Lopez de Arcaute y Lozano<sup>2</sup> · Stefanie Hanke<sup>2</sup> · Sebastian A. Kaiser<sup>1</sup>

Received: 15 June 2022 / Accepted: 10 October 2022 / Published online: 31 October 2022  
© The Author(s) 2022

## Abstract

Cavitation erosion is typically studied with ultrasonic sonotrodes. Only a few attempts have been made to study cavitation erosion of technical alloys on the level of repeated single bubbles. Such single cavitation bubbles can be induced by a focused laser pulse with high spatio-temporal repeatability. In this work, the surface damage caused by series of laser-induced single bubbles in water is observed with a light microscope in-situ between two successive bubbles. Polished samples from pure aluminum, an austenitic steel (316L, X2CrNiMo18-15-3), and a nickel aluminum bronze (CuAl10Ni5Fe5) were subjected to series of bubbles that typically had a maximum diameter of  $d=2.5$  mm and a non-dimensional stand-off distance  $\gamma=1.4$ . Via in-situ microscopy, the appearance of individual pits can be assigned to a specific, single bubble collapse event without removing the sample. Consistent with literature, for the chosen parameters the damaged region after many bubbles is circular, with individual pits that are deeper for aluminum than for the bronze and the steel. Additionally, our findings suggest that even high-strength materials can be damaged by the impact of just one single bubble, while not every single bubble causes a pit on the soft aluminum. From series of images after each bubble, the rate of pit accumulation was determined to be 2.6 pits/bubble for aluminum and around 0.3–0.5 pits/bubble for the two technical alloys.

**Keywords** In-situ microscopy · Cavitation erosion · Single-bubble cavitation · Wear testing

## 1 Introduction

Cavitation—the formation and collapse of gas bubbles in liquids—can, in the long term, damage the surfaces even of high-strength solid materials [1]. Beyond the unwanted effects, cavitation can also be useful, e.g., in the medical context [2, 3], particle synthesis [4], and surface cleaning [5, 6]. Either way, it is important to understand the mechanisms behind cavitation erosion. The cavitation resistance of materials is typically determined with ultrasonic sonotrodes according to ASTM G32 [7]. However, due to the multitude and stochasticity of these acoustically generated bubbles, the damage can generally not be assigned to individual bubble events. Alternatively, it is possible to generate single bubbles in a spatio-temporally precise and reproducible way via

focused laser pulses [8]. The focused light causes a breakthrough plasma from which a bubble of water vapor and other gases is formed [9, 10]. In addition to many studies on the fluid dynamics of the collapsing bubble [11–15], there is also work on the effect of such individual bubbles on a nearby deformable solid surface [16–19].

Various mechanisms have been identified as responsible for the damage of solid materials by cavitation. Their contribution to the resulting damage generally depends on the non-dimensional stand-off distance  $\gamma$  (the ratio of the distance  $d$  from the bubble center to surface and the maximum bubble radius  $r$ ) [18, 19]. Early work by Tomita and Shima identified several damage mechanisms in relatively soft materials [19]. Some are due to the liquid jet [18, 19] and the emission of shock waves during the bubble collapse [18–20]. Shear stress from wave propagation within the solid can also damage the surface [21]. Dular et. al exposed a laminated aluminum foil to single bubbles and observed the remaining plastic deformation in-situ [22]. They concluded that for bubbles very close to the surface the micro jet is the more pronounced mechanism whereas for bubble with  $\gamma > 0.5$  the collapsing rebound of the bubble close to the

✉ Jonas Kühlmann  
jonas.kuehlmann@uni-due.de

<sup>1</sup> Universität Duisburg-Essen, IVG - Reaktive Fluide,  
Carl-Benz-Str. 199, 47057 Duisburg, Germany

<sup>2</sup> Universität Duisburg-Essen, ITM - Werkstofftechnik,  
Lotharstraße 1, 47057 Duisburg, Germany

surface is more important [22]. However, with few exceptions, the solids used in these studies were soft materials, so that the deformation by a single bubble could be correlated with its dynamics. In a pioneering study, Phillip and Lauterborn [18] examined the damage from many single bubbles on technical alloys. It was found that the spatial damage patterns correspond to those on softer materials. But the individual pits were smaller, which was attributed to the higher yield strength of the materials. Our own previous work aimed to link the damage evolution on technical alloys caused by single bubbles to that in acoustic cavitation [23].

However, quite a gap remains between microscopically uncontrolled damage of technical alloys by acoustic cavitation and exactly reproducible loading of soft materials by single bubbles. To address this, we developed an optical arrangement that enables observing the surface of the sample during a running experiment. Near a sample immersed in water, series of single bubbles are created by focused laser pulses, and their effects are observed with an in-situ microscope. This method not only provides insight into the course of cavitation damage of technical materials but also can be used to evaluate the cavitation erosion resistance from the rate of single-bubble damage accumulation.

## 2 Methods and Materials

The formation of cavitation damage was investigated on a stainless steel (316L, X2CrNiMo18-15-3, 1.4441), a nickel aluminum bronze (NAB, CuAl10Ni5Fe5), and pure aluminum (Al 99,999%), the latter to make the connection with the more numerous experiments on softer materials. A more detailed description of the material properties can be found in [17, 23], and micrographs are shown in the Appendix. The samples were cylindrical with a diameter of 12 mm and a thickness of 8 mm and their surface was polished. The cavitation bubbles were created approximately above the center of the flat face of the cylindrical sample.

Figure 1 shows the optical arrangement. The experiment consists of three orthogonal optical trains at different wavelengths, one for pulsed-laser generation of a bubble, one for imaging the bubble dynamics, and a microscope viewing the sample surface in-situ. To generate bubbles, a 1064 nm nanosecond-pulsed Nd:YAG laser was focused into a cuvette filled with deionized water. First, the beam was expanded and passed an adjustable aperture. Two axicons then shaped the round transverse laser beam profile into a ring. This way the plasma breakdown is more likely to occur near to the beam waist [24–26]. Finally, the beam was focused into the water with an auxiliary lens and an aspheric lens, the former compensating for the refractive index of water that the latter was not designed for. The bubble dynamics were recorded orthogonal to the

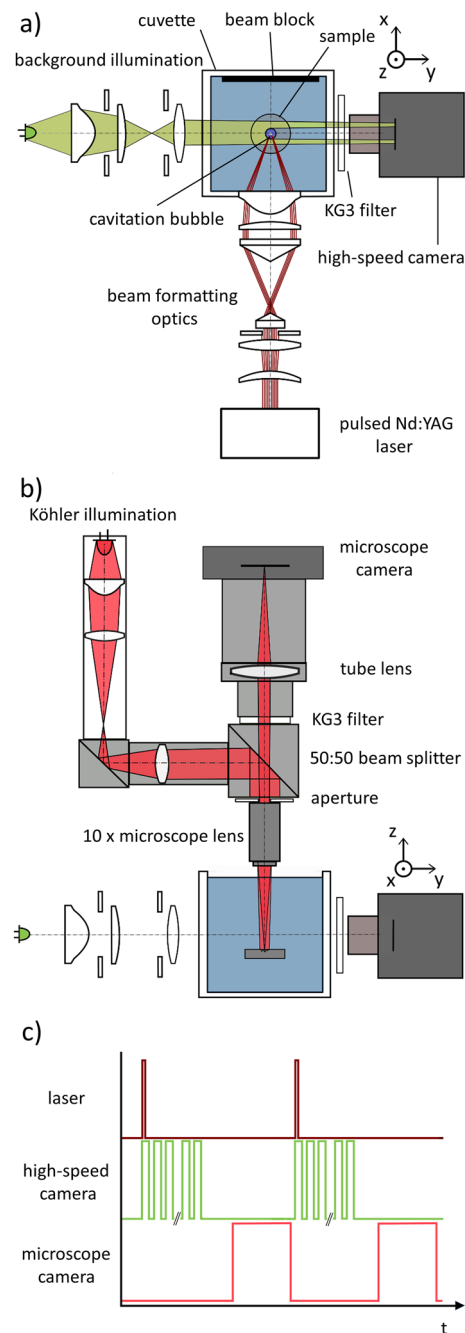


**Fig. 1** Schematic views of the experiment. **a** top view of single-bubble generation and detection, **b** side view of the in-situ microscope, **c** trigger sequence

direction of laser incidence. To that end, a Phantom VEO 710 high-speed camera imaged the shadow of the bubble backlit with an LED with a center wavelength of 505 nm. At 90 000 frames per second (fps),  $320 \times 180$  pixels were read with an exposure time of  $10 \mu\text{s}$ . Series of 100 frames (about 1 ms) captured the relevant part of each bubble's dynamics.

The microscope is shown in Fig. 1b. The sample surface, submersed about 20 mm below the water surface, was illuminated with an LED centered at 632 nm. A Mitutoyo Plan Apo 10× microscope objective lens and a Raynox DRC-250 tube lens provided a long working distance at a magnification of about six. To reduce aberrations caused by the water [20], a 6 mm aperture located just above the objective lens limited the numerical aperture of the objective to 0.14. This also increased the depth of field, advantageous for observing deep damage. The laser was triggered at a repetition rate of 1 Hz for experiments targeting the early damage formation and with 15 Hz for experiments with many successive cavitation bubbles. Schott KG3 filters protected the sensor of the microscope camera and that of the high-speed camera from elastically scattered laser light. In the microscope, a round region with a diameter of about 2300 camera pixels was illuminated, corresponding to about 2.5 mm on the sample surface. The images were taken 5 ms before each laser pulse (i.e., bubble), as shown in the trigger scheme in Fig. 1c. Alternatively, with the delay set to zero, the microscope recorded the plasma breakdown in the liquid, which was used for optimization of the beam formatting optics.

In addition to this reflected-light in-situ microscopy, which may be limited in resolution and contrast and is not quantitative, selected samples were also examined with two other microscopic techniques ex-situ after the experiment. Differential interference contrast (DIC) in an Olympus BX 41 microscope qualitatively visualized the surface texture, while a quantitative measurement of surface elevation was obtained with a NanoFocus  $\mu$ Surf confocal scanning microscope.

### 3 Results and Discussion

It is well-known that the dynamics of a bubble collapsing near a surface are strongly influenced by the stand-off distance  $\gamma$  [27, 28]. Most of the current experiments were performed at  $\gamma = 1.3$  to 1.4, a range for which a relatively complex damage pattern occurs, as will be seen below. An exemplary bubble collapse for  $\gamma = 1.4$  is shown in Fig. 2. As in all images in this paper, the laser is incident from the left. The first frame at  $t = -98 \mu\text{s}$  shows the plasma (whereas the central bright spot at later times is from the LED back-illumination) and the start of the formation of the bubble. After 98  $\mu\text{s}$  the bubble reaches its maximum diameter. It collapses towards the surface and is pierced by a downward liquid jet [28]. The rebound and the second collapse in Fig. 2 at 272  $\mu\text{s}$  and 380  $\mu\text{s}$ , respectively, occur in a toroidal shape very close to the solid surface. Note that the reflection of the bubble shadow on the polished sample surface helps locate the sample surface with respect to the bubble. The small dark spots throughout the image are attributed to bubbles

of dissolved gases that may not only stem from the air, but also possibly from the laser-induced breakdown plasma for the preceding bubbles.

The number of bubbles impacting on the surface is another important parameter. Previous works indicated that it may take tens of thousands of bubbles to induce substantial damage in technical alloys [8, 23]. In order to obtain an overview of the damage evolution, such experiments were also carried out. However, the current work focusses on the beginning of the damage evolution, and therefore most samples were exposed to less than 1000 cavitation bubbles.

Figure 3 shows three different microscope images of the cavitation damage on a 316L sample impacted by a series of 30 000 bubbles with a maximum diameter of 2.5 mm at  $\gamma = 1.4$ . The image taken by the in-situ microscope is shown in Fig. 3a. The other two, ex-situ images of the same damage, from confocal scanning microscopy (Fig. 3b) and a commercial light microscope with DIC (Fig. 3c), serve as a reference for the quality and informative value of the in-situ microscope images. The circular shape of the damaged region seen here is consistent with other works [16, 18]. There are both less damaged regions where individual pits can still be discerned, and a more severely damaged region. Thus, the quality of the images can be assessed in both of these damage scenarios, which may also be representative of earlier and later stages of local damage evolution.

Comparing Fig. 3a, c, the effects of aberrations caused by the 20 mm of water above the sample are visible as a slight blur in the in-situ image. But as far as the overview figure allows, all major features that can be seen in ex-situ can also be found in-situ. A more detailed ex-situ analysis can then complement that with quantitative measurements. For example, the confocal image in Fig. 3b shows that the depth of the most damaged region is 4  $\mu\text{m}$  and that of a typical single pit is about 0.25  $\mu\text{m}$ , consistent with our previous work with the same material [23]. This then can be linked to the corresponding contrast in the in-situ image.

Series of measurements were performed with selected stand-off distances. The in-situ images in Fig. 4 give a first overview of the stages of the damage processes for aluminum, 316L, and NAB. The experiments on aluminum were performed to link to the literature results on soft materials. The samples were successively exposed to 30 000 single cavitation bubbles for 316L and 50 000 for NAB. Images at 1 500, 3 000, and 14 400 bubbles are also shown in Fig. 4. Aluminum was exposed to a number of bubbles that induced similar cavitation damage as on the technical alloys, with images at 11, 24, 48, and 150 bubbles shown here. For all three materials, with an increasing number of bubbles an increase in the damage becomes visible. At all stages, most of the damage is in a ring-shaped area, best seen in the last images, and this is again consistent with the literature [16, 18]. The ring consists of smaller individual

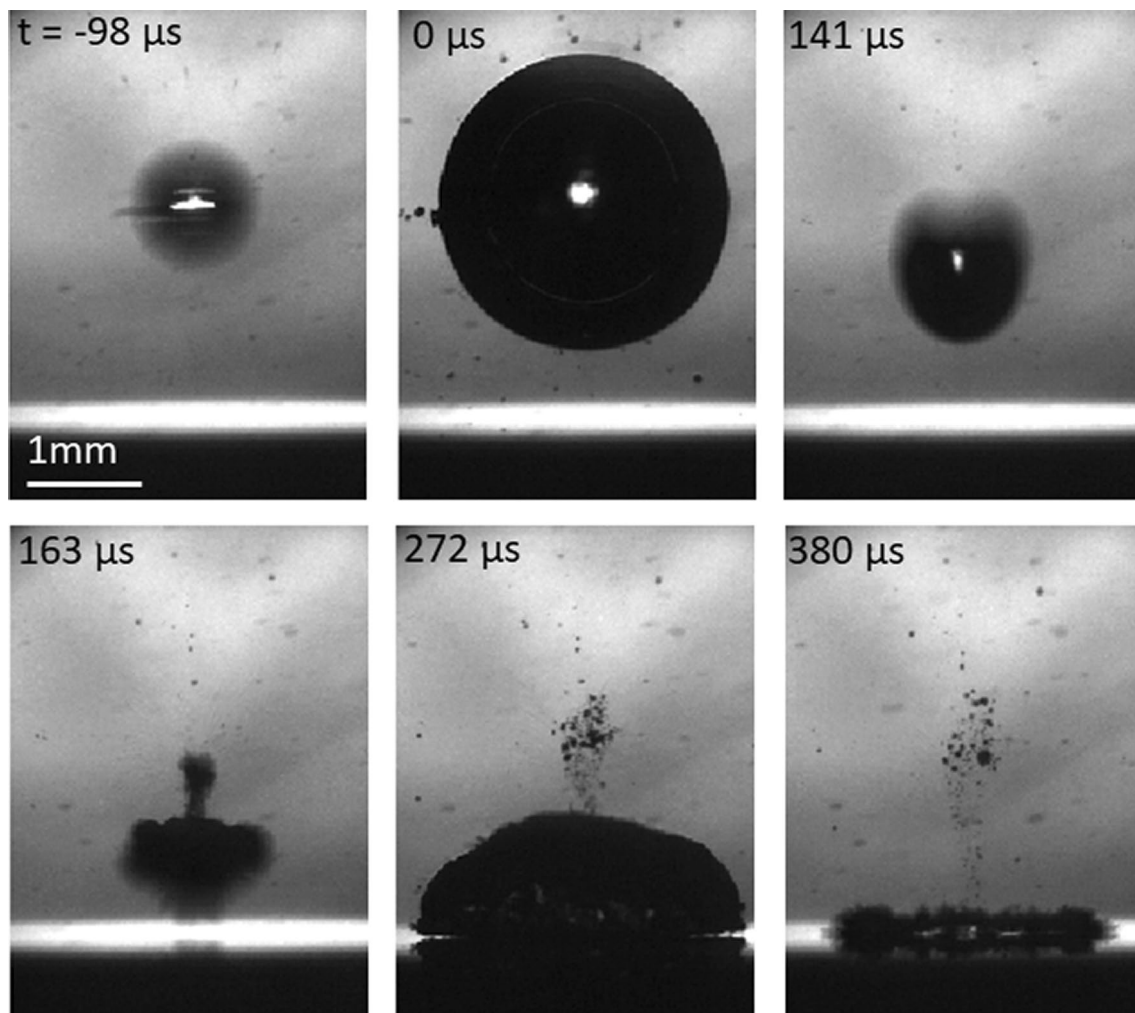


**Fig. 2** Selected frames from an example recording of the dynamics of a 2.5 mm diameter bubble at  $\gamma = 1.4$ . Time zero is defined here as the time of maximum bubble diameter. The laser incident is from the left

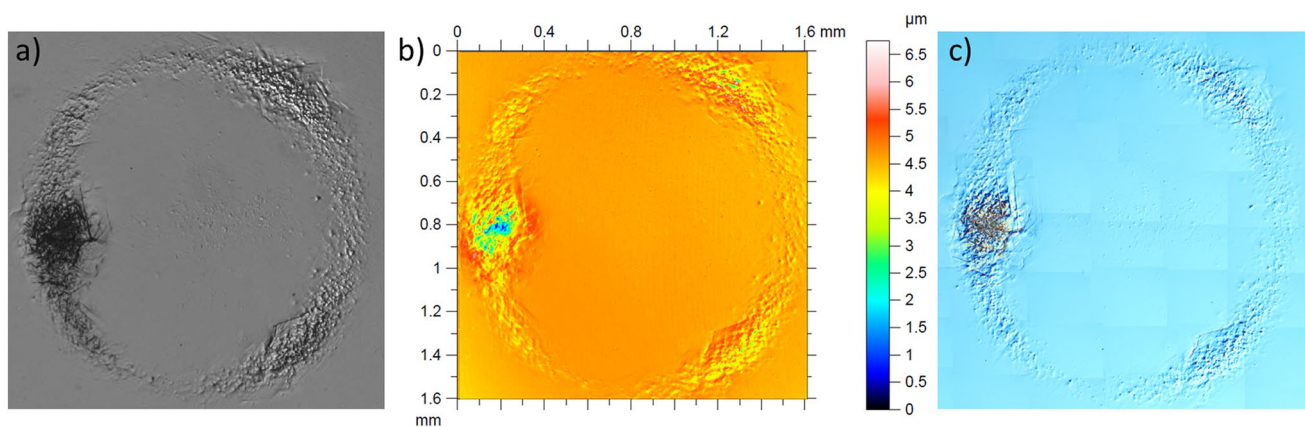


**Fig. 3** Comparison of an in-situ microscope image on 316L after 30 000 individual bubble impacts compared with the ex-situ imaging of the same damage. **a** in-situ image, **b** surface elevation from confocal

scanning, **c** DIC image, assembled from about 60 frames acquired with a 20 $\times$  objective. All images are shown at the same magnification, with the spatial scale given in **(b)**

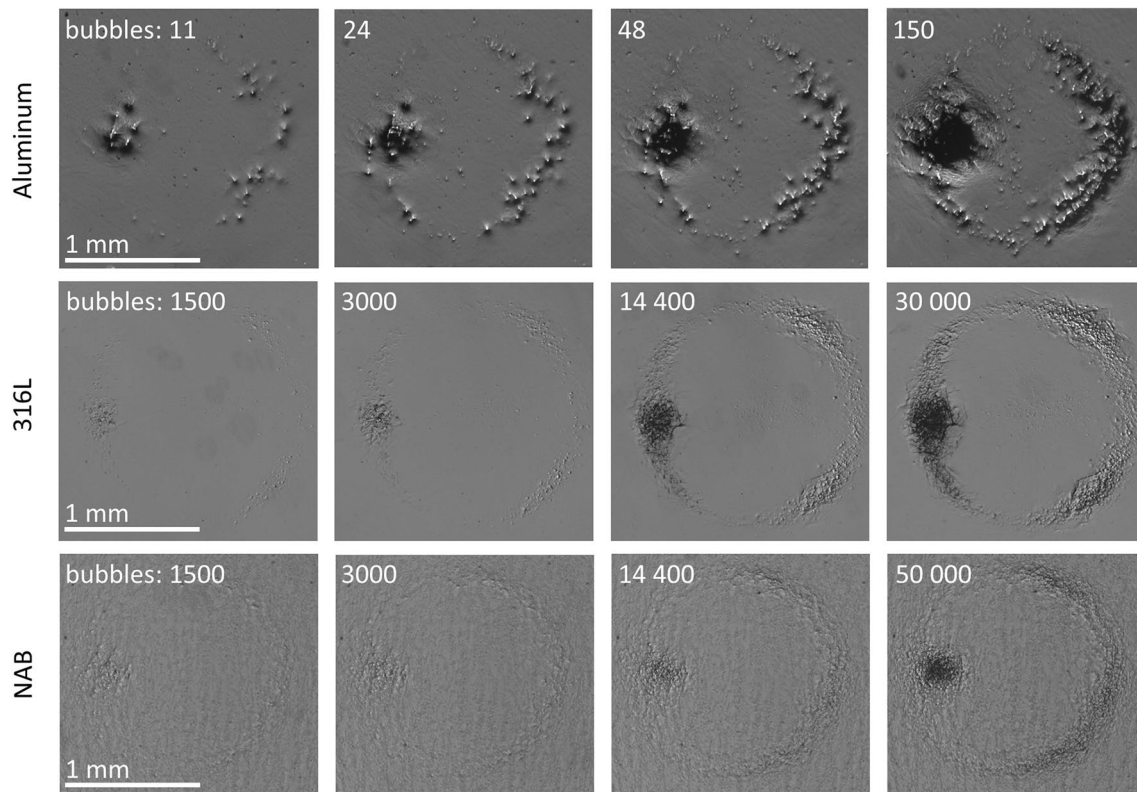


**Fig. 4** Damage evolution on aluminum (top), 316L (middle), and NAB (bottom) at  $\gamma=1.4$  and  $r=2.6$  mm bubble radius

pits. For aluminum, after 11 bubbles already more than 25 individual pits can be detected. This means that one bubble can cause more than two pits on aluminum. The damage evolution on the soft aluminum shows some differences to that on the harder two materials. Besides progressing much faster, the pits are bigger, and the area surrounding each pit appears more deformed.

Our findings are consistent with those of Philipp and Lauterborn [18] and Isslin et al. [16] in that they show an asymmetry in the otherwise ring-shaped damage patterns, with an area of more severe damage towards the direction of incoming laser light. This is most likely due to an asymmetry in the plasma breakdown [18], which is not spherical, but rather elongated and conical [29], as Fig. 2 at  $t=-98$   $\mu\text{s}$  indicates. Among all stand-off distances,  $\gamma=1.4$  creates the laterally most extended damage area, which may make the damage more prone to such asymmetries (see [18] for damage patterns with other stand-off distances). In fact, experiments with this  $\gamma$ -value can be used to detect plasma asymmetries that otherwise are difficult to visualize.

Among the two technical alloys, in good agreement with our previous work, NAB shows greater resistance to cavitation exposure than 316L in that the optically detected damage appears less severe after the same number of cavitation bubbles [23]. Also, the change in surface

damage appearance differs between 316L and NAB. The difference increases with the number of bubbles. For 316L, after 30 000 bubbles almost the full circumference of the ring-shaped damage displays pits. The damage concentration towards the incident beam appears very dark, indicative of its great depth. On the opposite half of the ring, two regions with less pronounced damage accumulation are recognizable (at approximately 1 and 5 o'clock). On NAB all these features appear less pronounced, and regions adjacent to the most damaged region on the side of the incident beam display almost no damage in these images. Furthermore, the surface of the NAB sample in general appears less smooth, showing small-scale grey variations in brightness in the image. This is caused by the complex microstructure in NAB, which contains both areas of high density of hard intermetallic phases, and others consisting mainly of softer Cu-rich solid-solution phase. A small difference in surface height between these different regions after polishing the sample surface causes the diffuse grey shading of the surface. The hard phases improve NAB's resistance to cavitation exposure by hindering plastic deformation and limiting pit dimensions. 316L on the other hand is a single-phase material, in which only grain boundaries and strain hardening limit pit formation by plastic deformation, which may act in NAB as well.

Therefore, damage appears less pronounced in NAB, consistent with previous findings [23]. While the collapsing bubbles clearly change the surface topology, it is not clear if conversely these changes in the surface influence the bubble dynamics and thus potentially the further damage progression. Recent studies show that purposeful texturing of the surface can lead to reduced cavitation erosion [30, 31]. It was suggested that a change in topology may

affect the primary dynamics of the bubble [31] as well as secondary phenomena during the collapse [30].

Figure 5 shows four microscope images from a 316L sample, taken after 0, 8, 9, and 100 bubble collapses, as well as a magnified region within each of these images. As discussed with Fig. 3, the dark, more or less diffuse spots that change position between images are shadows of small bubbles remaining after the preceding bubble collapse.

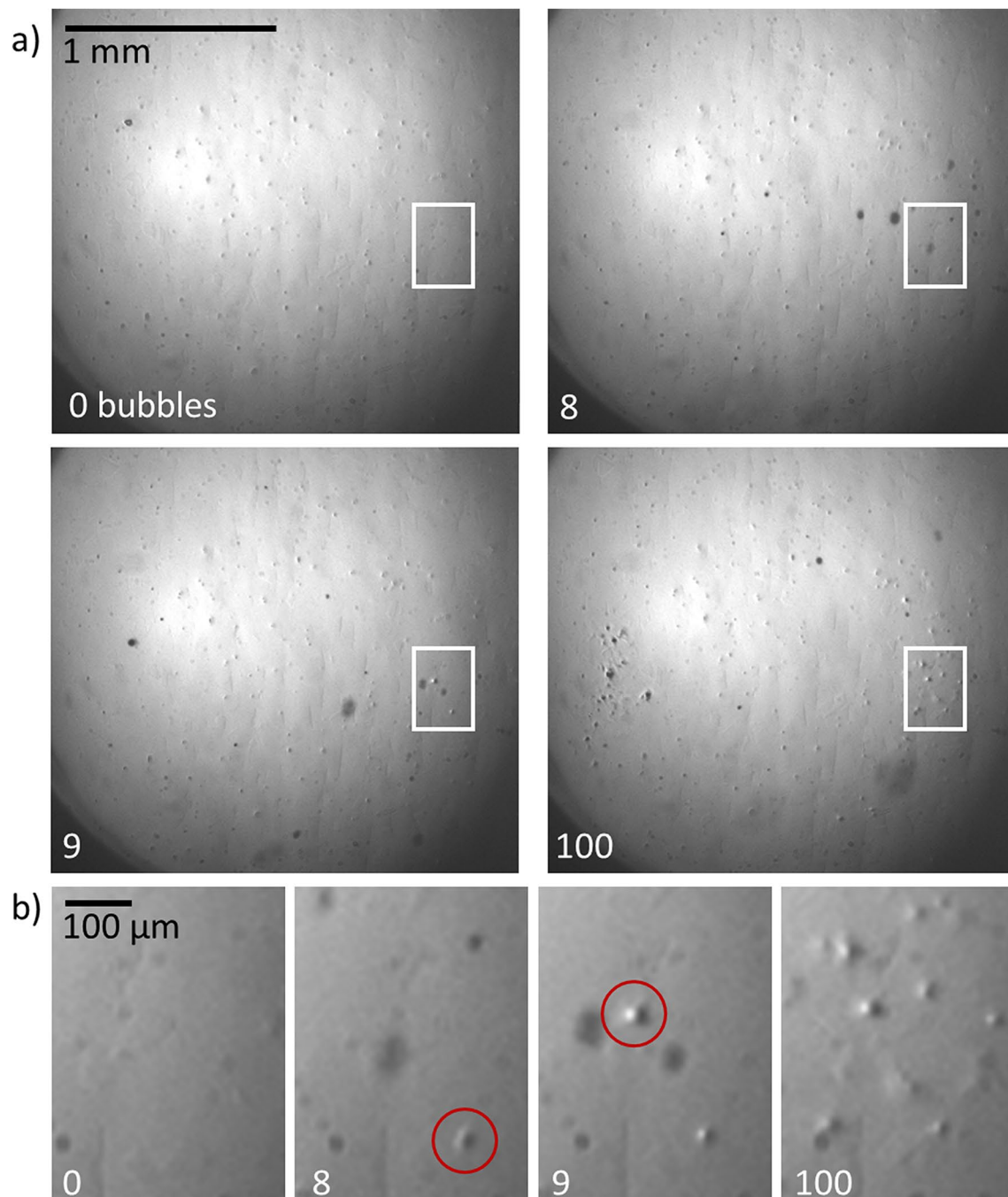


**Fig. 5** Damage formation on 316L at  $\gamma=1.4$  and 1.25 mm bubble radius. **a** full field of view, **b** magnified region corresponding to the white rectangle in (a). The red circles mark features discussed in the text

After the 8th bubble, the first pit appears, as marked in Fig. 5b. The next pit occurs already with the next (the 9th) bubble. This pit is then due to exactly the single preceding bubble. After 100 bubble collapses these two pits can still be identified. Note that the visual appearance of a given pit may change slightly between images. This is due to the fact that the water surface through which the images are taken is not perfectly still. The small pits that are the result of the bubble collapses later accumulate to form the larger ring structure as discussed above. As for the individual pits that now can be assigned to specific bubbles, we have not yet identified any feature in those particular bubble collapses that produce the pit in that particular spot. Nevertheless, the small size of the pit indicates that this damage might not have been caused by the first bubble collapse (for example, by the jet [8, 22]) but a smaller-scale event in the second toroidal-shaped collapse, as already suggested by other works [8, 22, 32].

Indeed, Fig. 6. shows that the damage ring is located under the second, toroidal bubble collapse. Still, it remains unclear what exactly caused a pit in a given spot. It may have been a particular, local feature of the bubble. An asymmetry in the torus of the second collapse can clearly be seen in Fig. 6 a–c. Regions on the ring displaying damage accumulation as described above (see Fig. 4) appear darker in the high-speed camera images, indicating the presence of more and possibly larger bubble structures. The shockwave emitted from the initial bubble might be a central part of the bubble dynamics as it has the potential to grow cavitation nuclei in the vicinity of the solid boundary [22, 32].

In Fig. 7 the damage progression is shown for  $\gamma = 1.7$  on NAB. For this stand-off distance less damage was observed than for  $\gamma = 1.4$ , as can be seen by comparison with Fig. 4 (NAB 14 400 bubbles). The first pit appeared after the 6th bubble, and two pits were caused by the 16th bubble collapse. Thus, even on technical materials, it is possible for one bubble collapse to create more than one pit. For  $\gamma = 1.7$  the damage pattern after many bubbles is not a ring but a smaller, central area that is again formed by smaller pits. The damage shape is consistent with measurements with this  $\gamma$  by Philipp and Lauterborn on a soft sample [18]. The last image in Fig. 7 shows that the first three pits are not clearly recognizable anymore at a count of 17 500 bubbles, because they are covered by further pits.

We see that for both technical alloys the initial surface damage begins after only a few bubbles—in fact, so few, that it seems likely that for a given sample already the first bubble may cause a pit. The cause of the pits seems to have a stochastic component, as neither their time of appearance nor their exact locations currently seem to be predictable, apart from the general location that is dependent on the stand-off distance  $\gamma$ .

To obtain a quantitative measure of early damage progression, we counted the pits after each bubble within a series. Pit counting was done by visual inspection, and the size and shape of the pit was disregarded. Figure 8 shows the result for series of 100 successive bubbles for the three materials, with two samples for NAB. Between zero and six additional pits are found after a single collapse. The slope of this pit count graph, approximated here as a

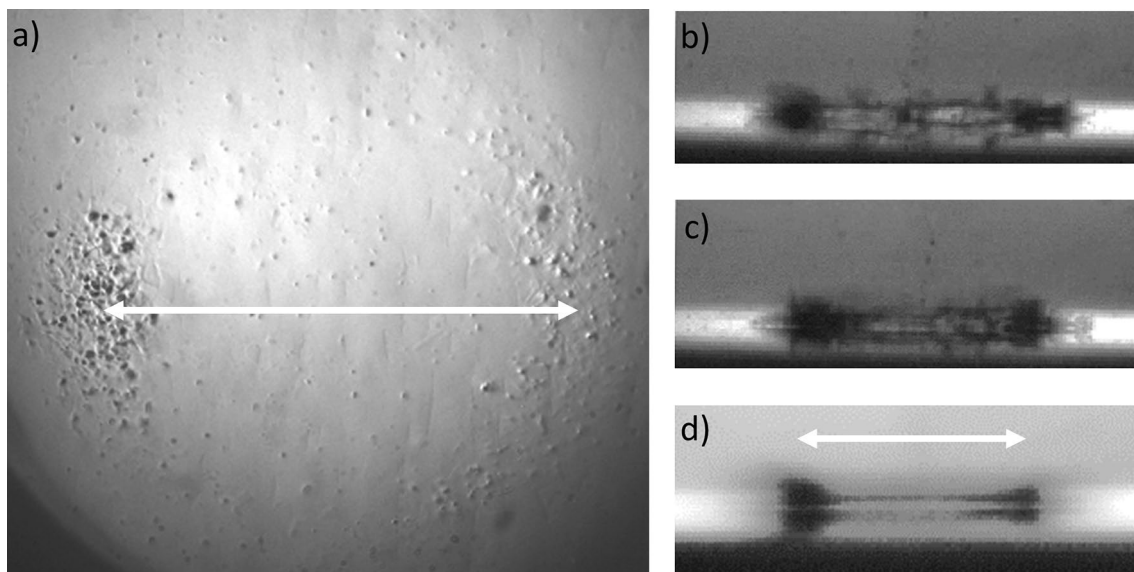


**Fig. 6** Relation of **a** the damaged region as seen by the in-situ microscope after 1000 bubbles and **b–c** the second collapse visualized with the high-speed camera. **b, c** are single shots of the second collapse

in selected bubbles, while **d** shows the mean of 200 collapses. The arrows in both images correspond to 1.55 mm. The images are from the same sample as those in Fig. 5

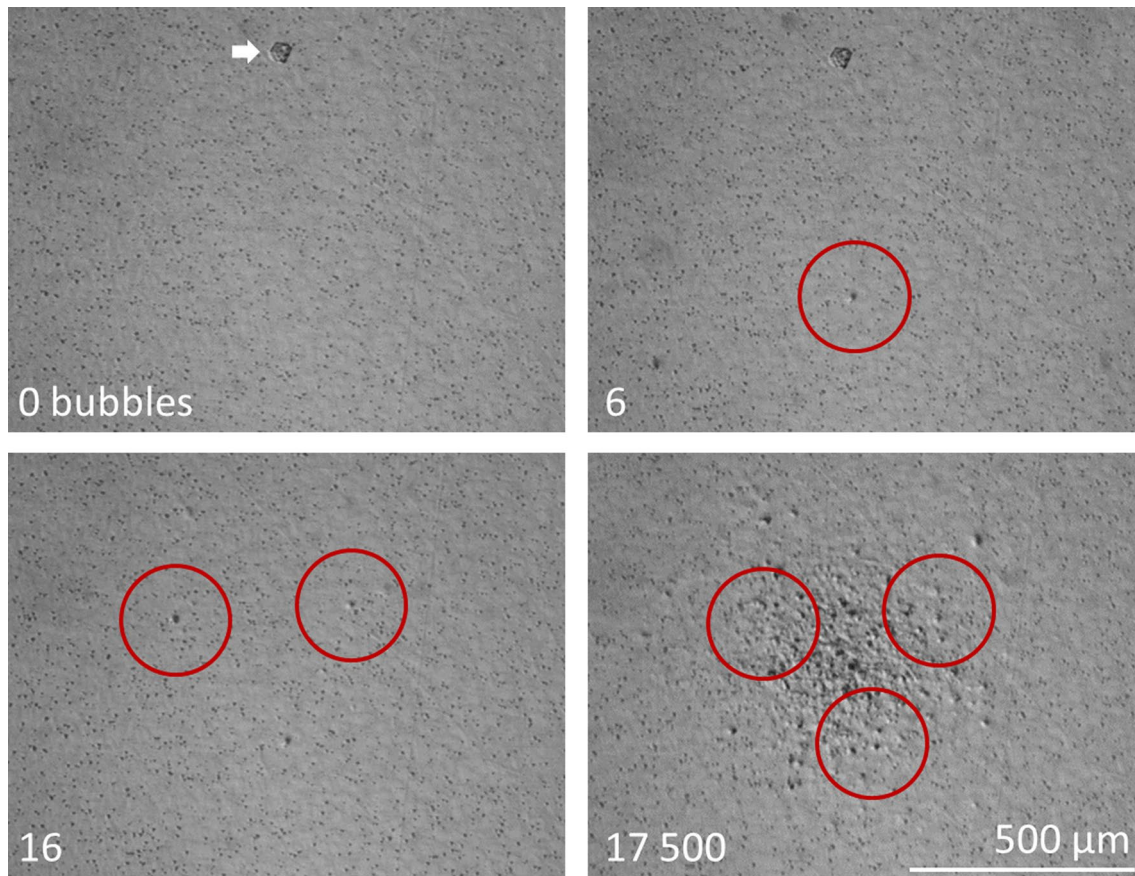


**Fig. 7** Early damage formation after 6 and 16 bubbles, and accumulated damage after 17 500 bubbles on NAB with  $\gamma=1.7$ . The circles mark features discussed in the text. The white arrow in image 0 marks

a feature that is an adhering particle of dirt that detached from the sample surface between the 6th and the 16th bubble

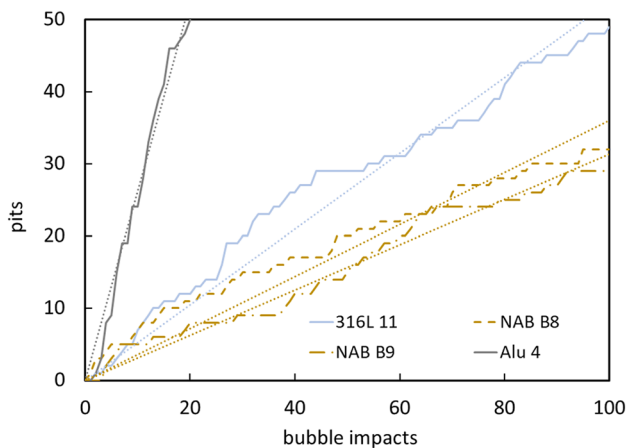


**Fig. 8** Pit count per bubble and linear fit of the pit count. For NAB, two samples were considered, as indicated in the legend after the material designation

linear fit through the origin to each data series, is then the series-mean pitting rate. The parameters of these experiments and the pitting rate are listed in Table 1. About 50 pits could be counted on a single sample before it became hard to distinguish overlapping pits. Beginning pit overlap may also be the reason why the slope of all traces decreases towards higher pit counts. The pitting rates have the same order among the materials as the corresponding material hardness, as does the maximum number of pits after a single-bubble collapse. After one collapse, 0–2 pits occurred on NAB, 0–3 on 316L, and 0–6 on aluminum. It is also remarkable that on one hand, even a soft material like aluminum did not show damage after every collapsing bubble. On the other hand, sample B8 from the hard NAB had a pit after the very first bubble. The two NAB samples differ slightly in their bubble parameters and in the pit count progression, but in this initial demonstration it is not clear if the difference is significant.



**Table 1** Parameters of the experiments and results of the pit counting presented in Fig. 8. The hardness was not measured on the samples used here, but on other samples from the same material and with the same processing

	NAB sample B8	NAB sample B9	316L sample 11	Aluminum sample 4
Hardness [HV 0.05]	201 ± 6		168 ± 6	22 ± 1
$\gamma$	1.36	1.28	1.36	1.30
Radius [mm]	1.23	1.3	1.36	1.25
Mean no. of pits/bubble	0.36	0.31	0.51	2.6
Min–max no. of pits/bubble	0–2	0–2	0–3	0–6

## 4 Conclusions

In this work, in-situ microscopy was established as a method for studying single-bubble induced cavitation damage. The basic idea is to generate successive single bubbles with a focused laser, and then take an in-situ microscope image of the surface after each bubble. The technique was tested for three different materials—pure aluminum, a stainless steel, and a nickel aluminum bronze—and was validated against established ex-situ microscopy techniques. The images from the in-situ microscope showed good general agreement with the ex-situ analysis. The damage patterns observed on the samples for the stand-off distances considered here are consistent with the much earlier work of Philipp and Lauterborn [18] as well as with more recent studies [18, 23]. For all three materials this pattern is formed out of an accumulation of smaller pits, each of which may be caused by events in the second collapse of the cavitation bubble. However, as expected, the rate of the damage progression greatly differed between the soft aluminum and the two harder technical alloys. The in-situ imaging shows that the response of the material surrounding the pits was different for the steel and the bronze.

The first onset of visible cavitation damage was investigated in more detail. With the in-situ surface microscopy it was possible to identify the appearance of individual pits and attribute them to a specific bubble. Somewhat surprisingly we found that even on the hardest test material, the bronze, the very first bubble can cause damage, and some bubbles even create two pits. Conversely, on the soft aluminum not every bubble causes a visible pit, even though most yield more than one. This bubble-by-bubble damage progression was quantified as a pitting rate by counting the pits over series of bubbles until they started to overlap often, which was the case at about 50 bubbles. Pit counting was done by visual inspection here, but should be amendable to automation, and could then be used for a systematic and statistically sound investigation of the onset of single-bubble cavitation damage. For prevention

of cavitation damage, it might be significant that there are bubble collapses that do not cause visible damage. From the current experiment, even though for each pit the corresponding bubble was recorded (in a side view) on a high-speed camera, we could not find an obvious connection between bubble dynamics and occurrence or exact location of a pit. If we could prevent whatever stochastic part of the bubble dynamics is responsible for the pits, that might prevent damage.

**Supplementary Information** The online version contains supplementary material available at <https://doi.org/10.1007/s11249-022-01665-5>.

**Acknowledgements** This research was funded by the German Research Foundation (DFG) under grant number 451715773.

**Author Contributions** All authors contributed to the study conception and design. Material preparation and the ex-situ analysis were performed by CLdeAyl. JK built the experimental apparatus, performed the experiments, and evaluated the data. The material science aspects of the study were mainly reviewed by SH, whereas SAK reviewed the experiment and the data processing. The first draft of the manuscript was written by JK and all authors commented on various versions of the manuscript. All authors read and approved the final manuscript.

**Funding** Open Access funding enabled and organized by Projekt DEAL. This research was funded by the German Research Foundation (DFG) under Grant Number 451715773.

## Declarations

**Competing Interests** The authors have no relevant financial or non-financial interests to disclose.

**Open Access** This article is licensed under a Creative Commons Attribution 4.0 International License, which permits use, sharing, adaptation, distribution and reproduction in any medium or format, as long as you give appropriate credit to the original author(s) and the source, provide a link to the Creative Commons licence, and indicate if changes were made. The images or other third party material in this article are included in the article's Creative Commons licence, unless indicated otherwise in a credit line to the material. If material is not included in the article's Creative Commons licence and your intended use is not permitted by statutory regulation or exceeds the permitted use, you will need to obtain permission directly from the copyright holder. To view a copy of this licence, visit <http://creativecommons.org/licenses/by/4.0/>.

## References

- Parsons, C.A., Cook, S.S.: Investigations into the causes of corrosion or erosion of propellers. *J. Am. Soc. Nav. Eng.* (1919). <https://doi.org/10.1111/j.1559-3584.1919.tb00807.x>
- Dijkink, R., Le Gac, S., Nijhuis, E., van den Berg, A., Vermes, I., Poot, A., Ohl, C.-D.: Controlled cavitation-cell interaction: trans-membrane transport and viability studies. *Phys. Med. Biol.* (2008). <https://doi.org/10.1088/0031-9155/53/2/006>
- Brennen, C.E.: Cavitation in medicine. *Interface focus* (2015). <https://doi.org/10.1098/rsfs.2015.0022>
- Barcikowski, S., Plech, A., Suslick, K.S., Vogel, A.: Materials synthesis in a bubble. *MRS Bull.* (2019). <https://doi.org/10.1557/mrs.2019.107>
- Ohl, C.-D., Arora, M., Dijkink, R., Janve, V., Lohse, D.: Surface cleaning from laser-induced cavitation bubbles. *Appl. Phys. Lett.* (2006). <https://doi.org/10.1063/1.2337506>
- Reuter, F., Lauterborn, S., Mettin, R., Lauterborn, W.: Membrane cleaning with ultrasonically driven bubbles. *Ultrason. Sonochem.* (2017). <https://doi.org/10.1016/j.ultrsonch.2016.12.012>
- G02 Committee: Test Method for Cavitation Erosion Using Vibratory Apparatus. ASTM International, West Conshohocken, PA
- Lauterborn, W.: High-speed photography of laser-induced breakdown in liquids. *Appl. Phys. Lett.* (1972). <https://doi.org/10.1063/1.1654204>
- Brewer, R.G., Rieckhoff, K.E.: Stimulated Brillouin scattering in liquids. *Phys. Rev. Lett.* (1964). <https://doi.org/10.1103/PhysRevLett.13.334>
- Noack, J., Vogel, A.: Laser-induced plasma formation in water at nanosecond to femtosecond time scales: calculation of thresholds, absorption coefficients, and energy density. *IEEE J. Quant. Elec.* (1999). <https://doi.org/10.1109/3.777215>
- Akhatov, I., Lindau, O., Topolnikov, A., Mettin, R., Vakhitova, N., Lauterborn, W.: Collapse and rebound of a laser-induced cavitation bubble. *Phys. Fluids* (2001). <https://doi.org/10.1063/1.1401810>
- Obreschkow, D., Tinguely, M., Dorsaz, N., Kobel, P., de Bosset, A., Farhat, M.: The quest for the most spherical bubble: experimental setup and data overview. *Exp. Fluids* (2013). <https://doi.org/10.1007/s00348-013-1503-9>
- Gonzalez-Avila, S.R., Klaseboer, E., Khoo, B.C.O., Ohl, C.-D.: Cavitation bubble dynamics in a liquid gap of variable height. *J. Fluid Mech.* (2011). <https://doi.org/10.1017/jfm.2011.212>
- Reuter, F., Gonzalez-Avila, S.R., Mettin, R., Ohl, C.-D.: Flow fields and vortex dynamics of bubbles collapsing near a solid boundary. *Phys. Rev. Fluids* (2017). <https://doi.org/10.1103/PhysRevFluids.2.064202>
- Brujan, E.A., Keen, G.S., Vogel, A., Blake, J.R.: The final stage of the collapse of a cavitation bubble close to a rigid boundary. *Phys. Fluids* (2002). <https://doi.org/10.1063/1.1421102>
- Isselin, J.-C., Alloncle, A.-P., Autric, M.: On laser induced single bubble near a solid boundary: contribution to the understanding of erosion phenomena. *J. Appl. Phys.* (1998). <https://doi.org/10.1063/1.368841>
- Sagar, H.J., Hanke, S., Underberg, M., Feng, C., el Moctar, O., Kaiser, S.A.: Experimental and numerical investigation of damage on an aluminum surface by single-bubble cavitation. *Mats. Perf. Charact.* (2018). <https://doi.org/10.1520/MPC20180038>
- Philipp, A., Lauterborn, W.: Cavitation erosion by single laser-produced bubbles. *J. Fluid Mech.* (1998). <https://doi.org/10.1017/S0022112098008738>
- Tomita, Y., Shima, A.: Mechanisms of impulsive pressure generation and damage pit formation by bubble collapse. *J. Fluid Mech.* (1986). <https://doi.org/10.1017/S0022112086000745>
- Lauterborn, W., Vogel, A.: Shock wave emission by laser generated bubbles. In: Delale, C.F. (ed.) *Bubble Dynamics and Shock Waves*, pp. 67–103. Springer, Berlin, Heidelberg (2013)
- Hsiao, C.-T., Jayaprakash, A., Kapahi, A., Choi, J.-K., Chahine, G.L.: Modelling of material pitting from cavitation bubble collapse. *J. Fluid Mech.* (2014). <https://doi.org/10.1017/jfm.2014.394>
- Dular, M., Požar, T., Zevnik, J., Petkovšek, R.: High speed observation of damage created by a collapse of a single cavitation bubble. *Wear* (2019). <https://doi.org/10.1016/j.wear.2018.11.004>
- Hanke, S., Kaiser, S.A.: Comparison of damage mechanisms: Acoustic cavitation versus series of single laser-induced bubbles. *Wear* (2021). <https://doi.org/10.1016/j.wear.2021.203641>
- Fuchs, U., Braun, D., Wickenhagen, S.: Beam shaping concepts with aspheric surfaces. In: Forbes, A., Lizotte, T.E. (eds.) *Laser Beam Shaping XVI. SPIE Optical Engineering + Applications*. Optica publishing group, San Diego, California, United States (2015)
- Tian, Y., Xue, B., Song, J., Lu, Y., Zheng, R.: Stabilization of laser-induced plasma in bulk water using large focusing angle. *Appl. Phys. Lett.* (2016). <https://doi.org/10.1063/1.4960711>
- Sinibaldi, G., Occhicone, A., Alves Pereira, F., Caprini, D., Marino, L., Michelotti, F., Casciola, C.M.: Laser induced cavitation: plasma generation and breakdown shockwave. *Phys. Fluids* (2019). <https://doi.org/10.1063/1.5119794>
- Blake, J.R., Gibson, D.C.: Cavitation bubbles near boundaries. *Annu. Rev. Fluid Mech.* (1987). <https://doi.org/10.1146/annurev.fl.19.010187.000531>
- Blake, J.R., Leppinen, D.M., Wang, Q.: Cavitation and bubble dynamics: the Kelvin impulse and its applications. *Interface focus* (2015). <https://doi.org/10.1098/rsfs.2015.0017>
- Vogel, A., Busch, S., Parltz, U.: Shock wave emission and cavitation bubble generation by picosecond and nanosecond optical breakdown in water. *J. Acoust. Soc. Am.* (1996). <https://doi.org/10.1121/1.415878>
- Gonzalez-Parra, J.C., Robles, V., Devia-Cruz, L.F., Rodriguez-Beltran, R.I., Cuando-Espitia, N., Camacho-Lopez, S., Aguilar, G.: Mitigation of cavitation erosion using laser-induced periodic surface structures. *Surf. Interfaces* (2022). <https://doi.org/10.1016/j.surfin.2021.101692>
- Kadivar, E., el Moctar, O., Skoda, R., Löschner, U.: Experimental study of the control of cavitation-induced erosion created by collapse of single bubbles using a micro structured riblet. *Wear* (2021). <https://doi.org/10.1016/j.wear.2021.204087>
- sDular, M., Stoffel, B., Širok, B.: Development of a cavitation erosion model. *Wear* (2006). <https://doi.org/10.1016/j.wear.2006.01.020>

**Publisher's Note** Springer Nature remains neutral with regard to jurisdictional claims in published maps and institutional affiliations.